INTERNATIONAL JOURNAL FOR NUMERICAL METHODS IN FLUIDS
Int. J. Numer. Meth. Fluids 2000; **33**: 535–557

Control of Navier–Stokes equations by means of mode reduction

H. M. Park* and M. W. Lee

Department of Chemical Engineering, Sogang University, Seoul, Republic of Korea

SUMMARY

In a previous work (Park HM, Lee MW. An efficient method of solving the Navier–Stokes equation for the flow control. *International Journal of Numerical Methods in Engineering* 1998; **41**: 1131–1151), the authors proposed an efficient method of solving the Navier–Stokes equations by reducing their number of modes. Employing the empirical eigenfunctions of the Karhunen–Loève decomposition as basis functions of a Galerkin procedure, one can *a priori* limit the function space considered to the smallest linear sub-space that is sufficient to describe the observed phenomena, and consequently, reduce the Navier–Stokes equations defined on a complicated geometry to a set of ordinary differential equations with a minimum degree of freedom. In the present work, we apply this technique, termed the Karhunen–Loève Galerkin procedure, to a pointwise control problem of Navier–Stokes equations. The Karhunen–Loève Galerkin procedure is found to be much more efficient than the traditional method, such as finite difference method in obtaining optimal control profiles when the minimization of the objective function has been done by using a conjugate gradient method. Copyright © 2000 John Wiley & Sons, Ltd.

KEY WORDS: control of Navier–Stokes equations; Karhunen–Loève Galerkin procedure; mode reduction

1. INTRODUCTION

Optimal control theory of viscous fluid motion has important applications in engineering and science. Our ability to actively or passively manipulate a flow field to effect a desired change is of immense technological importance. Some applications of control of fluid flows in industrial processes may be the viscous drag reduction to minimize the drag force on a submerged body, the control of mixing patterns in chemical reactors to enhance the reactor performance, separation postponement, lift enhancement, or noise suppression.

* Correspondence to: Department of Chemical Engineering, Sogang University, Shinsoo-Dong, Mapo-Gu, Seoul, Republic of Korea.

Received 18 February 1999

With the problems of flow control, one usually encounters substantial difficulties because of the mathematical complexities of the Navier–Stokes equations. The Navier–Stokes equations, which are a distributed parameter system, has an almost infinite degree of freedom with strong non-linearity. Although computational tools that combine modern computational fluid dynamics and rigorous optimization methods have been recently applied to the flow control problems [2,3], these analyses are usually very complicated mathematically, and there are still technical difficulties to be overcome before they become practical design tools. One of the most important prerequisites for the successful application of advanced control techniques to fluid flows of industrial importance is the development of a reliable dynamic model, with small degrees of freedom, that is not mathematically complicated but is still applicable to the cases of irregular domains.

Until now, several research groups [4,5] have used the Karhunen–Loève decomposition as a procedure for computation of coherent structures (empirical eigenfunctions) in turbulence from experimental or numerical data of flow fields. Usually these empirical eigenfunctions have been used to interpret the statistical characteristics of the turbulent flow. Furthermore, by employing these empirical eigenfunctions and introducing additional drastic approximations to the Navier–Stokes equations, they could derive reduced order models for turbulent flows [6] or transitional flows [7]. These reduced order models [6,7] do not simulate the fluid flows exactly, but are found to approximately reproduce some interesting characteristics of turbulence or transitional flows, such as intermittency and bifurcation sequences. Although these reduced order models are not exact, there have been some attempts to apply the dynamical system methodology to these low order models to control fluid flows [8]. Because the original Karhunen–Loève decomposition technique [5–7] is applicable only to stationary stochastic fields, such as turbulence or oscillatory transitional flows, it could not be employed in the rigorous control schemes of fluid flows. But recent works [1,9,10] have extended the Karhunen–Loève decomposition to the analysis of non-stationary, non-homogeneous deterministic as well as stochastic fields, and allowed the derivation of rigorous reduced order models that simulate the given systems almost exactly. This extension of the original Karhunen–Loève decomposition is called the Karhunen–Loève Galerkin procedure [1,9,10], and can be adopted in rigorous implementation of modern control schemes for viscous fluid flows.

Previously, we have explained the Karhunen–Loève Galerkin procedure, which can reduce the Navier–Stokes equations defined on a irregular geometry to a faithful low dimensional dynamic model, and have suggested it as an efficient computational tool for flow control or optimization [1]. In the present work, we examine the feasibility and efficiency of the Karhunen–Loève Galerkin procedure as a method of solving the pointwise control problems of the Navier–Stokes equation.

The detail of the Karhunen–Loève Galerkin procedure, which is a Galerkin method employing the empirical eigenfunctions of the Karhunen–Loève decomposition, is well documented in Park and Lee [1] and Park and Cho [9,10]. In the following sections, we shall describe the system and governing equations with relevant boundary conditions. Following that, the procedure of construction of empirical eigenfunctions shall be explained in detail, and the low dimensional dynamic model for the system under consideration shall be suggested. Finally, the problem of pointwise control of the viscous fluid flow shall be solved by employing

the Navier–Stokes equation and the low dimensional dynamic model, respectively, and the efficiency and accuracy of the Karhunen–Loève Galerkin procedure for the solution of control problems of viscous fluid flow shall be assessed. In both cases, the minimization of the objective function has been performed by means of a conjugate gradient method.

2. THEORY

2.1. The system and governing equation

We consider a viscous incompressible fluid flow in a grooved cavity as shown in Figure 1. The flow is induced not only by the lid velocity, but also by a forcing located at the position (0.625, 0.25) indicated in Figure 1(a). The point source forcing is approximated mathematically by the function $f(t)\delta_{10}(x-0.625)\delta_{10}(z-0.25)$ where $\delta_n(x)$ is defined by:

$$\delta_n(x) = \frac{n}{2\cosh^2(nx)} \tag{1}$$

and $f(t)$ is an arbitrary time-varying function. This function $\delta_n(x)$ becomes the Dirac delta function $\delta(x)$ as n approaches infinity. The shape and strength of the point source forcing is plotted in Figure 1(b). The unsteady flow field of the system is obtained by solving the following incompressible Navier–Stokes equation with forcing.

$$\rho\left(\frac{\partial \boldsymbol{v}}{\partial t} + \boldsymbol{v}\cdot\nabla\boldsymbol{v}\right) = -\nabla P + \mu\nabla^2\boldsymbol{v} + \boldsymbol{i}\rho f(t)\delta_{10}(x-x^*)\delta_{10}(z-z^*) \tag{2}$$

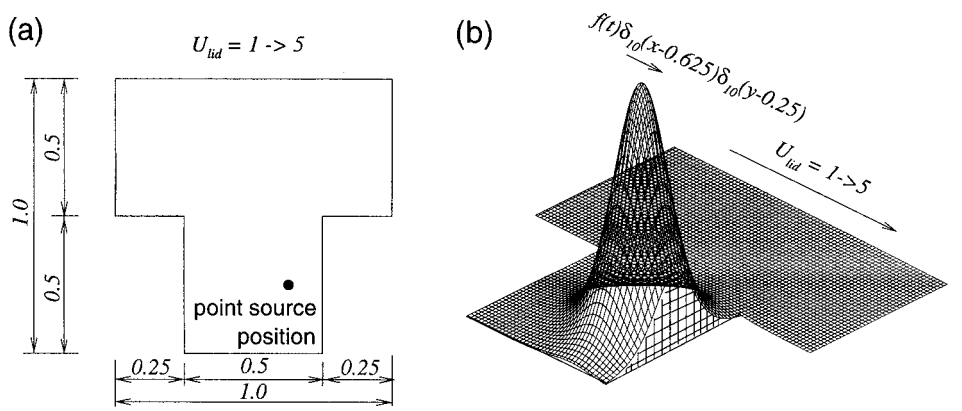

Figure 1. (a) System under consideration. The flow is induced by both the lid velocity undergoing a step change from 1 to 5, and a point source located within the domain. (b) The shape and strength of the point source.

$$\nabla \cdot \boldsymbol{v} = 0 \tag{3}$$

where $\boldsymbol{v}$ is the velocity vector, P the pressure, ρ the density ($=1$), μ the viscosity ($=1$), $\boldsymbol{i}$ is the unit vector in the x-direction, $x^* = 0.625$ and $z^* = 0.25$. For the specific case under consideration, Equations (2) and (3) may be rewritten as follows.

$$\rho\left(\frac{\partial u}{\partial t} + u\frac{\partial u}{\partial x} + w\frac{\partial u}{\partial z}\right) = -\frac{\partial P}{\partial x} + \mu\left(\frac{\partial^2}{\partial x^2} + \frac{\partial^2}{\partial z^2}\right)u + \rho f(t)\delta_{10}(x - x^*)\delta_{10}(z - z^*) \tag{4}$$

$$\rho\left(\frac{\partial w}{\partial t} + u\frac{\partial w}{\partial x} + w\frac{\partial w}{\partial z}\right) = -\frac{\partial P}{\partial x} + \mu\left(\frac{\partial^2}{\partial x^2} + \frac{\partial^2}{\partial z^2}\right)w \tag{5}$$

$$\frac{\partial u}{\partial x} + \frac{\partial w}{\partial z} = 0 \tag{6}$$

where u and w are the x- and z-components of the velocity field $\boldsymbol{v}$, respectively. The relevant initial and boundary conditions are follows:

Initial conditions

$$\boldsymbol{v}(x, z, t = 0) \text{ the steady velocity field with the lid velocity} = 1.0 \text{ and } f(t) = 0 \tag{7}$$

Boundary conditions

$$\cdot z = 1.0 \text{ (upper boundary)}; u = 5, w = 0 \tag{8}$$

$$\cdot \text{ all other boundaries; } u = w = 0 \tag{9}$$

The problem at hand is that of controlling the system above to produce a state variable $\boldsymbol{v}(\boldsymbol{x}, T)$, at the final time T, that is as close as possible to a target flow field $\boldsymbol{v}_T(\boldsymbol{x})$. We aim at achieving this goal through a pointwise control $f(t)\delta_{10}(x - x^*)\delta_{10}(z - z^*)$, which appears as a source or sink in Equation (4), in the spatial domain. Our concern is to achieve the goal while minimizing the cost of control $f(t)$. This suggests the problem

$$\min\ J(f) \tag{10}$$

where

$$J(f) = \frac{1}{2}\int_\Omega (\boldsymbol{v}(\boldsymbol{x}, T) - \boldsymbol{v}_T(\boldsymbol{x}, T))^2\, \mathrm{d}\Omega + \frac{\epsilon}{2}\int_0^T f(t)^2\, \mathrm{d}t \tag{11}$$

and ϵ is a small positive constant. To ensure that the target $\boldsymbol{v}_T(\boldsymbol{x})$ is a reachable state, we determine $\boldsymbol{v}_T(\boldsymbol{x})$ by integrating Equations (4)–(6) with a given function $f(t)$, and set $\boldsymbol{v}_T(\boldsymbol{x}) = \boldsymbol{v}(\boldsymbol{x}, t = T)$. In the present work, we consider two different target functions determined by integrating Equations (4)–(6) with the following controls.

$$\text{(Case a)} \qquad f(t) = \begin{cases} 2000\,t & \text{if } 0 \le t \le 0.05 \\ 2000(0.1 - t) & \text{if } 0.05 \le t \le 0.1 \end{cases} \tag{12a}$$

$$\text{(Case b)} \qquad f(t) = 50\left(1 + \sin\frac{2\pi t}{T}\right) \quad \text{for } 0 \le t \le 0.1 \tag{12b}$$

where $T = 0.1$. Each of these controls and corresponding target function $\boldsymbol{v}_T(\boldsymbol{x})$ are depicted in Figure 2(a) and (b) and Figure 3(a) and (b), respectively. In Figure 2(b) and Figure 3(b), the solid line is used for the positive values and the dotted line for the negative values of the stream function.

2.2. Construction of empirical eigenfunctions

Before applying the Karhunen–Loève Galerkin procedure to reduce the degree of freedom of the system, we need a set of empirical eigenfunctions which capture the system behaviour satisfactorily, at least for the ranges of possible variation of the control variable $f(t)$. These useful eigenfunctions can only be obtained from an ensemble of snapshots which are representative of the system characteristics [1,9,10]. The low dimensional dynamic model to be used in the solution of optimal control problem should predict the velocity profile $\boldsymbol{v}(\boldsymbol{x}, t)$ exactly for various trajectories of $f(t)$ that include not only the optimal trajectory, but also other trajectories appearing during the iterative minimization of the objective function (Equation (11)) by means of the conjugate gradient method. Assuming that the controls $f(t)$ appearing during the iterative procedure may be represented as linear combinations of sinusoidal modes (i.e. a Fourier series representation), with the highest frequency $w_{\max} = 10$, we

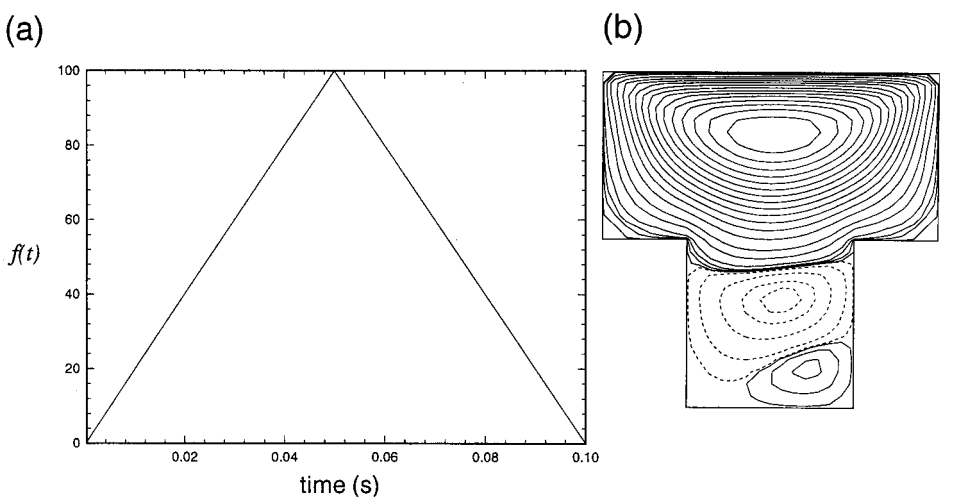

Figure 2. (a) The control given by Equation (12a). (b) Target velocity field $\boldsymbol{v}_T(\boldsymbol{x})$ determined by Equation (12a).

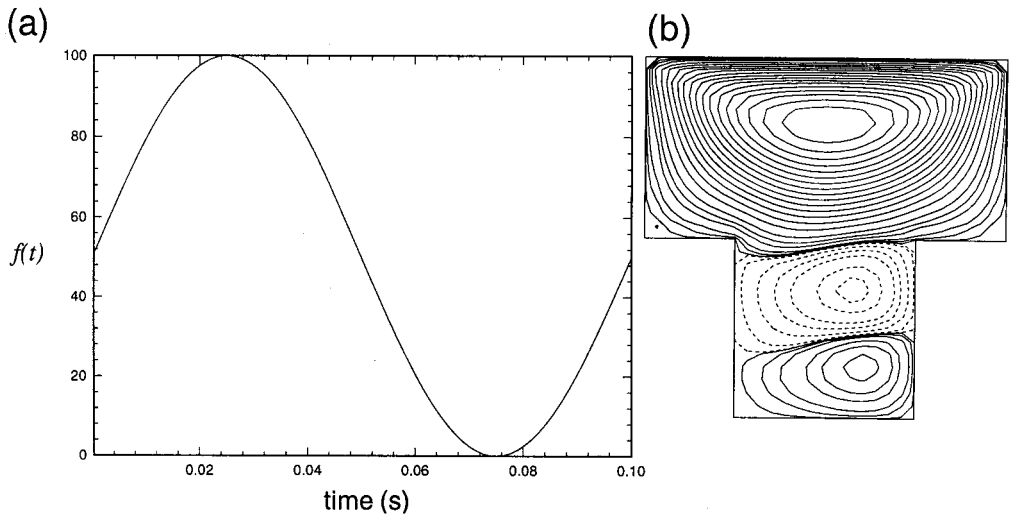

Figure 3. (a) The control given by Equation (12b). (b) Target velocity field $\boldsymbol{v}_T(\boldsymbol{x})$ determined by Equation (12b).

pick up $f(t) = 100$ and $f(t) = 50(1 + \sin(2\pi w_{\max} t/T))$ as the control trajectories to generate snapshots of $\{\boldsymbol{v}_n\}$. We have found that the snapshots obtained with the controls of intermediate frequencies are encompassed by this set of snapshots $\{\boldsymbol{v}_n\}$ obtained with the control of the lowest frequency ($f(t) = 100$) and with the control of the highest frequency ($f(t) = 50(1 + \sin(2\pi w_{\max} t/T))$). Thus, Equations (4)–(6) are solved with $f(t) = 100$ and the resulting transient velocity fields $\boldsymbol{v}(\boldsymbol{x}, t)$ are recorded at a constant time interval to generate 500 snapshots. Similarly, with $f(t) = 50(1 + \sin(2\pi t/T))$, we generate 500 snapshots. As explained in Park and Lee [1], it is necessary to make these snapshots satisfy homogeneous boundary conditions. For this purpose, we obtain the steady flow field $\boldsymbol{v}_r(\boldsymbol{x})$ by solving the following set of equations:

$$\rho \boldsymbol{v}_r \cdot \nabla \boldsymbol{v}_r = -\nabla P_r + \mu \nabla^2 \boldsymbol{v}_r \tag{13}$$

$$\nabla \cdot \boldsymbol{v}_r = 0 \tag{14}$$

with the following boundary conditions, where the x- and z-components of the $\boldsymbol{v}_r$ are denoted as u_r and w_r:

- at the top boundary; $u_r = \alpha_i$, $w_r = 0$ (15)
- at all other boundaries; $u_r = w_r = 0$ (16)

Here α_i is the lid velocity at $t \leq 0$, i.e. 1, and the value of the lid velocity imposed during the process ($t > 0$), α_f, is taken to be 5. Then each velocity field of the following set given by

$$\left(\boldsymbol{v}_n - \frac{\alpha_f}{\alpha_i} \boldsymbol{v}_r \right), \qquad n = 1, 2, \ldots, 1000 \tag{17}$$

satisfies homogeneous boundary conditions, i.e. all components of the velocity vanish at the boundary. To these 1000 snapshots satisfying homogeneous boundary conditions, we apply the Karhunen–Loève decomposition technique to get empirical eigenfunctions in the order of their importance in characterizing the system. Figure 4(a)–(h) shows the 1st, the 2nd, the 3rd and the 4th eigenfunctions, with the corresponding normalized eigenvalues $\lambda_1 = 0.823306$, $\lambda_2 = 0.161588$, $\lambda_3 = 1.06908 \times 10^{-2}$, $\lambda_4 = 2.66563 \times 10^{-3}$, respectively. Also shown in Figure 5(a)–(d) are typical eigenfunctions with smaller eigenvalues, i.e. the 9th, the 10th, the 11th and the 12th eigenfunctions, with the corresponding normalized eigenvalues, $\lambda_9 = 4.10828 \times 10^{-5}$, $\lambda_{10} = 1.08621 \times 10^{-5}$, $\lambda_{11} = 3.99717 \times 10^{-6}$, $\lambda_{12} = 1.47815 \times 10^{-6}$. Figure 4(a)–(d) reveals that the empirical eigenfunctions with large eigenvalues represent the large scale structures of the velocity field $\boldsymbol{v}$. On the contrary, from Figure 5(a)–(d), we find that eigenfunctions with small eigenvalues represent the small scale structures caused by the pointwise forcing and the system boundaries.

2.3. The low dimensional dynamic model

In this section, we develop working equations for the low dimensional dynamic model of the system that is to be used later in the solution of optimal control problem. As the first step of the Karhunen–Loève Galerkin procedure, which is a Galerkin method employing the above empirical eigenfunctions as basis functions, we represent the velocity field $\boldsymbol{v}(\boldsymbol{x}, t)$ as a linear combination of empirical eigenfunctions as follows:

$$\boldsymbol{v}(x, t) = \sum_{i=1}^{M} a_i(t)\phi_i(\boldsymbol{x}) + \beta \boldsymbol{v}_r(\boldsymbol{x}) \tag{18}$$

where ϕ_i is the ith empirical eigenfunction, $a_i(t)$ is the corresponding spectral coefficient, $\beta = \alpha/\alpha_i$, where α is the lid velocity which changes from α_i to α_f at $t = 0$, and M is the total number of empirical eigenfunctions employed in the Karhunen–Loève Galerkin procedure. The residual may be expressed as:

$$\boldsymbol{R} \equiv \frac{\partial \boldsymbol{v}}{\partial t} + \boldsymbol{v} \cdot \nabla \boldsymbol{v} + \nabla \frac{P}{\rho} - \nu \nabla^2 \boldsymbol{v} - if(t)\delta_{10}(x - x^*)\delta_{10}(z - z^*) \tag{19}$$

where $\nu \equiv \mu/\rho$. Applying the Galerkin principle, which enforces the residual to be orthogonal to each of the basis functions,

$$\int_\Omega \boldsymbol{R} \cdot \phi_i \, \mathrm{d}\Omega = 0 \qquad (i = 1, 2, \ldots, M) \tag{20}$$

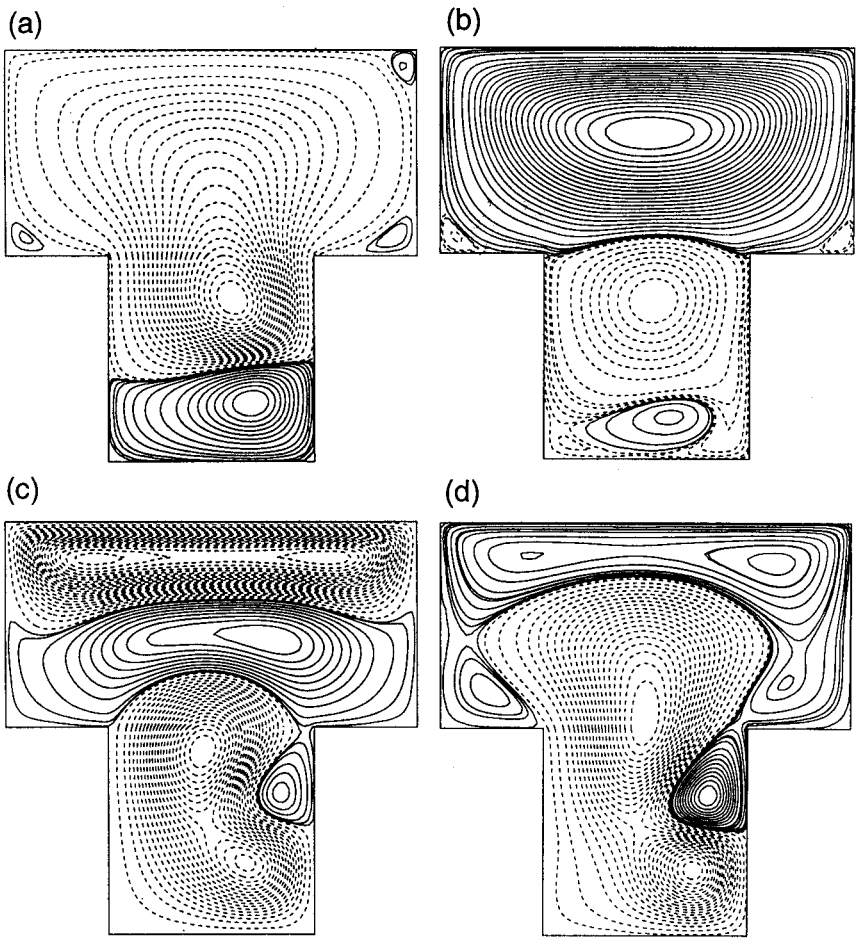

Figure 4. Some dominant empirical eigenfunctions with large eigenvalues. (a) The 1st eigenfunction. (b) The 2nd eigenfunction. (c) The 3rd eigenfunction. (d) The 4th eigenfunction.

the Equations (4)–(6) are reduced to the following set of non-linear ordinary differential equations [1].

$$M_k \frac{\mathrm{d}a_k}{\mathrm{d}t} = -\nu \sum_{l=1}^{M} a_l H_{kl} - \sum_{l=1}^{M}\sum_{m=1}^{M} a_l a_m Q_{klm} - \beta \sum_{l=1}^{M} a_l R_{kl} - \beta(\beta-1)C_k - N_k \frac{\mathrm{d}\beta}{\mathrm{d}t} + f(t)S_k \tag{21a}$$

with

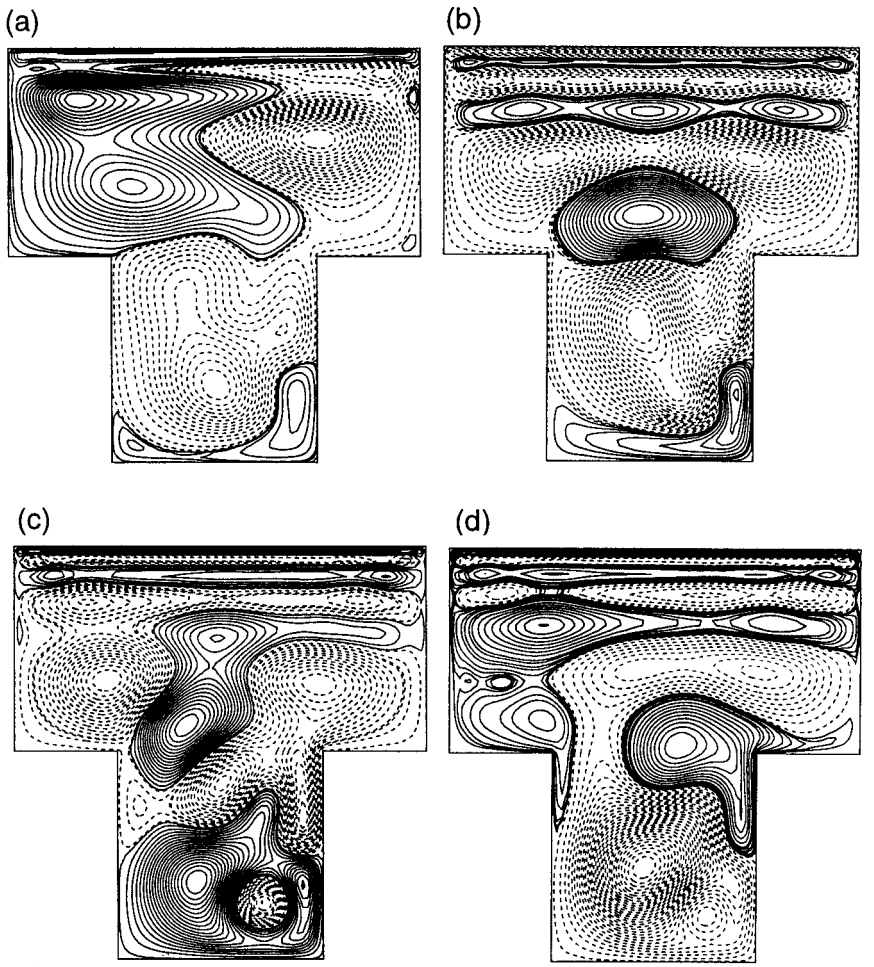

Figure 5. Some typical empirical eigenfunctions with small eigenvalues. (a) The 9th eigenfunction. (b) The 10th eigenfunction. (c) The 11th eigenfunction. (d) The 12th eigenfunction.

$$a_k(t=0) = \frac{\displaystyle\int_\Omega (\boldsymbol{v}(x,\, t=0) - \beta \boldsymbol{v}_r)\cdot \phi_k \, \mathrm{d}\Omega}{\displaystyle\int_\Omega \phi_k \cdot \phi_k \, \mathrm{d}\Omega} \tag{21b}$$

The coefficients in Equation (21a) may be expressed in terms of the x- and z-components of the eigenfunctions, ϕ_k^u and ϕ_k^w, as follows:

$$M_k \equiv \int_\Omega (\phi_k^u)^2 + (\phi_k^w)^2 \, \mathrm{d}\Omega \tag{22}$$

$$N_k \equiv \int_\Omega (\phi_k^u u_r + \phi_k^w w_r) \, \mathrm{d}\Omega \tag{23}$$

$$H_{kl} \equiv \int_\Omega \left(\frac{\partial \phi_k^u}{\partial x} \frac{\partial \phi_l^u}{\partial x} + \frac{\partial \phi_k^u}{\partial z} \frac{\partial \phi_l^u}{\partial z} + \frac{\partial \phi_k^w}{\partial x} \frac{\partial \phi_l^w}{\partial x} + \frac{\partial \phi_k^w}{\partial z} \frac{\partial \phi_l^w}{\partial z} \right) \mathrm{d}\Omega \tag{24}$$

$$Q_{klm} \equiv \int_\Omega \phi_k^u \left(\phi_l^u \frac{\partial \phi_m^u}{\partial x} + \phi_l^w \frac{\partial \phi_m^u}{\partial z} \right) + \phi_k^w \left(\phi_l^u \frac{\partial \phi_m^w}{\partial x} + \phi_l^w \frac{\partial \phi_m^w}{\partial z} \right) \mathrm{d}\Omega \tag{25}$$

$$\begin{aligned} R_{kl} \equiv \int_\Omega & \phi_k^u \left(\phi_l^u \frac{\partial u_r}{\partial x} + u_r \frac{\partial \phi_l^u}{\partial x} + \phi_l^w \frac{\partial u_r}{\partial z} + w_r \frac{\partial \phi_l^u}{\partial z} \right) \\ & + \phi_k^w \left(\phi_l^u \frac{\partial w_r}{\partial x} + u_r \frac{\partial \phi_l^w}{\partial x} + \phi_l^w \frac{\partial w_r}{\partial z} + w_r \frac{\partial \phi_l^w}{\partial z} \right) \mathrm{d}\Omega \end{aligned} \tag{26}$$

$$C_k \equiv \int_\Omega \phi_k^u \left(u_r \frac{\partial u_r}{\partial x} + w_r \frac{\partial u_r}{\partial z} \right) + \phi_k^w \left(u_r \frac{\partial w_r}{\partial x} + w_r \frac{\partial w_r}{\partial z} \right) \mathrm{d}\Omega \tag{27}$$

$$S_k \equiv \int_\Omega \phi_k^u \delta_{10}(x - x^*) \delta_{10}(z - z^*) \, \mathrm{d}\Omega \tag{28}$$

where u_r and w_r are the x- and z-components of the reference velocity vector $\boldsymbol{v}_r(\boldsymbol{x})$. Equation (21) is a set of ordinary differential equations, which may be solved by using the Adams–Bashforth method for the non-linear terms, and the Crank–Nicolson method for the linear terms. The performance of the low dimensional dynamic model (Equation (21)) is evaluated by comparing its solution with the finite difference solutions of Equations (4)–(6), which is regarded as the exact solution when the number of grids adopted is (80×80) for a given control $f(t)$. Usually, the relative error of the low dimensional dynamic model decreases as the number of eigenfunctions employed increases up to the optimal number of empirical eigenfunctions. However, further increase of number of eigenfunctions beyond the optimal number deteriorates accuracy because the eigenfunctions with very small eigenvalues are contaminated with round-off errors. The optimal number of empirical eigenfunctions is found to be 12, and thus, we are going to employ 12 eigenfuntions for the construction of the low dimensional dynamic model in the present work. Figure 6(a)–(b) depict a comparison of velocity components obtained by the Karhunen–Loève Galerkin procedure with those by the finite difference method at specific locations indicated in each figure when $f(t) = 50(1 + \sin(10\pi t/T))$. Figure 6(a) shows the x-component velocity u, while Figure 6(b) is for the z-component w. It is shown that the exact solution by the finite difference method, and the solution from the low dimensional dynamic model of the Karhunen–Loève Galerkin procedure, are almost the same at every point investigated.

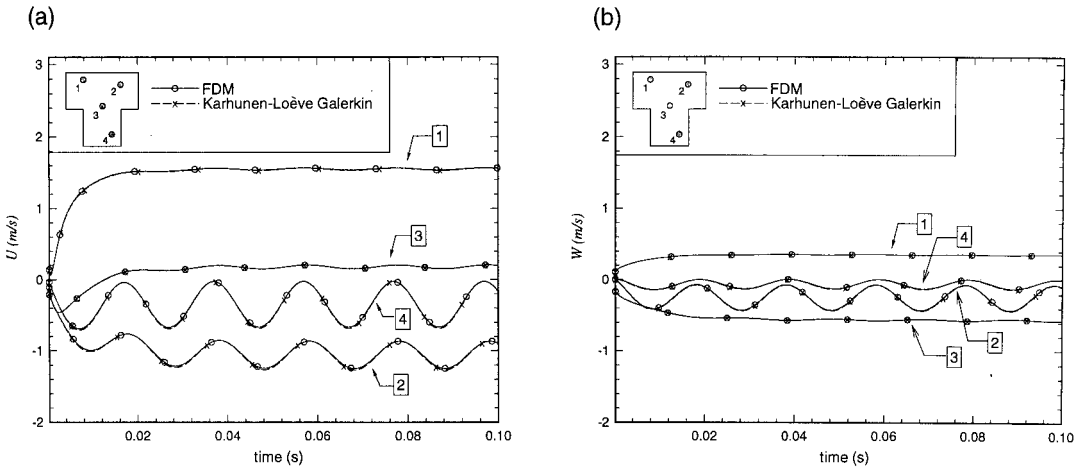

Figure 6. The temporal variation of velocity components selected points indicated in the figures when $f(t) = 50(1 + \sin(10\pi t/T))$. (a) x-component of the velocity vector, u. (b) z-component of the velocity vector, w.

2.4. Solution of optimal control problems employing the original partial differential equation

Before presenting the algorithm for solving optimal control problems employing the low dimensional dynamic model, we first describe how to solve the same problems by the finite difference solution of the original Navier–Stokes equation.

To minimize the objective function (Equation (11)), we need the gradient of J, ∇J, which is defined by

$$\delta J(f) = \int_0^T \nabla J \delta f \, \mathrm{d}t \tag{29}$$

where T, the final time, is 0.1 s. The function ∇J can be obtained by introducing an adjoint variables $\boldsymbol{\xi}(\boldsymbol{x}, t)$ and $q(\boldsymbol{x}, t)$, and rewriting the objective function as follows:

$$\begin{aligned} J(f) = {} & \frac{1}{2}\int_\Omega (\boldsymbol{v}(\boldsymbol{x}, T) - \boldsymbol{v}_T(\boldsymbol{x}))^2 \, \mathrm{d}\Omega + \frac{\epsilon}{2}\int_0^T f(t)^2 \, \mathrm{d}t \\ & - \int_0^T \int_\Omega \boldsymbol{\xi} \cdot \left[\frac{\partial v}{\partial t} + \boldsymbol{v} \cdot \nabla \boldsymbol{v} + \nabla \frac{P}{\rho} - \nu \nabla^2 \boldsymbol{v} + \boldsymbol{i} f(t) \delta_{10}(x - x^*) \delta_{10}(z - z^*) \right] \mathrm{d}\Omega \, \mathrm{d}t \\ & + \int_0^T \int_\Omega q(\nabla \cdot \boldsymbol{v}) \, \mathrm{d}\Omega \, \mathrm{d}t \end{aligned} \tag{30}$$

The variation of J, δJ, is then given by the following equation:

$$\delta J(f) = \int_0^T f\delta f \, \mathrm{d}t + \int_\Omega (\boldsymbol{v}(\boldsymbol{x}, T) - \boldsymbol{v}_T(\boldsymbol{x}))\cdot\delta\boldsymbol{v}(\boldsymbol{x}, T)\, \mathrm{d}\Omega - \int_0^T \int_\Omega \delta\boldsymbol{v}_t\cdot\boldsymbol{\xi}\, \mathrm{d}\Omega\, \mathrm{d}t$$
$$- \int_0^T \int_\Omega (\delta\boldsymbol{v}\cdot\nabla\boldsymbol{v})\cdot\boldsymbol{\xi}\, \mathrm{d}\Omega\, \mathrm{d}t - \int_0^T \int_\Omega (\boldsymbol{v}\cdot\nabla(\delta\boldsymbol{v}))\cdot\boldsymbol{\xi}\, \mathrm{d}\Omega\, \mathrm{d}t - \int_0^T \int_\Omega (\nabla\delta P/\rho)\cdot\boldsymbol{\xi}\, \mathrm{d}\Omega\, \mathrm{d}t$$
$$+ \nu \int_0^T \int_\Omega (\nabla^2\delta\boldsymbol{v})\cdot\boldsymbol{\xi}\, \mathrm{d}\Omega\, \mathrm{d}t - \int_0^T \delta f(t) \int_\Omega \delta_{10}(x - x^*)\delta_{10}(z - z^*)\xi^x(\boldsymbol{x}, t)\, \mathrm{d}\Omega\, \mathrm{d}t$$
$$+ \int_0^T \int_\Omega q(\nabla\cdot\delta\boldsymbol{v})\, \mathrm{d}\Omega\, \mathrm{d}t \tag{31}$$

where $\boldsymbol{\xi} = (\xi_x, \xi_z)$. Integrating δJ by parts, both in space and time, and exploiting the initial and boundary conditions for $\boldsymbol{v}$ and $\delta\boldsymbol{v}$, the gradient of J and ∇J in Equation (29) is found to be as follows:

$$\nabla J = f(t) - \int_\Omega \delta_{10}(x - x^*)\delta_{10}(z - z^*)\xi^x(x, z, t)\, \mathrm{d}\Omega \tag{32}$$

while the adjoint variables $\boldsymbol{\xi} = (\xi^x, \xi^z)$ and q must satisfy:

$$\frac{\partial\boldsymbol{\xi}}{\partial t} - \boldsymbol{\xi}\cdot(\nabla\boldsymbol{v})^T + \boldsymbol{v}\cdot\nabla\boldsymbol{\xi} = \nabla q - \nu\nabla^2\boldsymbol{\xi} \tag{33}$$

$$\nabla\cdot\boldsymbol{\xi} = 0 \tag{34}$$

with the starting condition

$$\boldsymbol{\xi}(\boldsymbol{x}, t = T) = \boldsymbol{v}(\boldsymbol{x}, T) - \boldsymbol{v}_T(\boldsymbol{x}) \tag{35}$$

and boundary conditions

$$\boldsymbol{\xi}(\boldsymbol{x}, t) = 0 \quad \text{on } \partial\Omega \tag{36}$$

The set of Equations (33)–(36) can be solved by means of the simple algorithm which is adopted for the solution of the state Equations (4)–(6). The Fletcher–Reeves method [11], which is one of the conjugate gradient methods, is successfully applied to the minimization of the objective function, using the gradient J determined by Equation (32). The search direction or the conjugate direction at the first step is determined by:

$$d^0(t) = \nabla J(t) = f(t) - \int_\Omega \delta_{10}(x - x^*)\delta_{10}(z - z^*)\xi^x(x, z, t)\, \mathrm{d}\Omega \tag{37}$$

Beginning the second iteration step, the conjugate direction is given by:

$$d^n(t) = \nabla J^n(t) + \gamma^n d^{n-1}(t) \tag{38}$$

where

$$\gamma^n = \frac{\int_0^T (\nabla J^n(t))^2 \, \mathrm{d}t}{\int_0^T (\nabla J^{n-1}(t))^2 \, \mathrm{d}t} \tag{39}$$

and n is the iteration number. The optimal step length ρ^n in the direction of d^n is obtained by minimizing $J(f^n - \rho^n d^n)$ with respect to ρ^n. Formally, $J(f^n - \rho^n d^n)$ is expressed as:

$$J(f^n - \rho^n d^n) = \frac{1}{2} \int_\Omega (\boldsymbol{v}(\boldsymbol{x}, T, f^n - \rho^n d^n) - \boldsymbol{v}_T(\boldsymbol{x}))^2 \, \mathrm{d}\Omega + \frac{\epsilon}{2} \int_0^T (f^n - \rho^n d^n)^2 \, \mathrm{d}t \tag{40}$$

The directional derivative of $\boldsymbol{v}$ at f in the direction of d, denoted as $\delta \boldsymbol{v}$, is defined by

$$\delta \boldsymbol{v} = \lim_{\epsilon \to 0} \frac{\boldsymbol{v}(f + \epsilon d) - \boldsymbol{v}(f)}{\epsilon} \tag{41}$$

Then, the term $\boldsymbol{v}(\boldsymbol{x}, T, f^n - \rho^n d^n)$ in Equation (40) is approximated by

$$\boldsymbol{v}(\boldsymbol{x}, T, f^n - \rho^n d^n) = \boldsymbol{v} - (\delta \boldsymbol{v}) \rho^n \tag{42}$$

Substituting Equation (42) into Equation (40) and partially differentiating it with respect to ρ^n, and setting the resulting equation equal to zero, the value ρ^n that minimizes $J(f^n - \rho^n d^n)$ is obtained as

$$\rho^n = \frac{\delta J^n}{K^n} \tag{43a}$$

where

$$K^n \equiv \int_\Omega \delta \boldsymbol{v}(\boldsymbol{x}, T, d) \cdot \delta \boldsymbol{v}(\boldsymbol{x}, T, d) \, \mathrm{d}\Omega + \epsilon \int_0^T d^2 \, \mathrm{d}t \tag{43b}$$

and

$$\delta J^n \equiv \int_\Omega (\boldsymbol{v}(\boldsymbol{x}, T) - \boldsymbol{v}_T(\boldsymbol{x})) \cdot \delta \boldsymbol{v}(\boldsymbol{x}, T) \mathrm{d}\Omega + \epsilon \int_0^T f(t) d(t) \, \mathrm{d}t \tag{43c}$$

The updated control $f^{n+1}(t)$ is obtained as

$$f^{n+1}(t) = f^n(t) - \rho^n d^n(t) \tag{44}$$

The sensitivity equation which determines $\delta \boldsymbol{v}$ is given as follows:

$$\frac{\partial}{\partial t}\delta\boldsymbol{v} + \delta\boldsymbol{v}\cdot\nabla\boldsymbol{v} + \boldsymbol{v}\cdot(\nabla\delta\boldsymbol{v}) = -\nabla\frac{\delta P}{\rho} + \nu\nabla^2\delta\boldsymbol{v} - \boldsymbol{i}\delta f\delta_{10}(x - x^*)\delta_{10}(z - z^*) \tag{45}$$

$$\nabla\cdot\delta\boldsymbol{v} = 0 \tag{46}$$

The relevant initial and boundary conditions are

$$\delta\boldsymbol{v}(\boldsymbol{x}, t = 0) = 0 \tag{47a}$$

$$\delta\boldsymbol{v} = 0 \quad \text{at all boundaries} \tag{47b}$$

Equations (45)–(47) can also be solved by using the simple algorithm. The present algorithm is summarized below.

1. Assume $f(t)$ and calculate the flow field $\boldsymbol{v}(\boldsymbol{x}, t)$ by means of Equations (4)–(6).
2. Solve the adjoint problem (Equations (33)–(36)).
3. ∇J is determined by Equation (32).
4. The conjugate direction $d^n(t)$ is given by Equation (38) with γ^n determined by Equation (39).
5. Solve the sensitivity Equations (45)–(47).
6. The step length in the conjugate direction $d^n(t)$ is determined by Equation (43(a)–(c)).
7. The updated control is obtained by Equation (44).
8. Repeat the above procedure until convergence.

2.5. Solution of optimal control problems employing the low dimensional dynamic model of the Karhunen–Loève Galerkin procedure

Employing the low dimensional dynamic model Equation (21) obtained by means of the Karhunen–Loève Galerkin procedure, one can also find the optimal control $f(t)$ that minimizes the objective function (11). The degree of freedom of Equation (21) is only 12, whereas the degree of freedom of the original partial differential equation, which is equivalent to the grid number in the finite difference approximation $\times 3$ (i.e. u, w, P), is about 2×10^4. The difference in degree of freedom between the low dimensional dynamic models and the original partial differential equations shall become much larger as the dimensionality of the problem change from two-dimensional to three-dimensional. Therefore, the procedure of optimal control problem employing the low-dimensional dynamic model is predestined to be much faster than that employing the original non-linear partial differential equation.

The objective function (Equation (11)) may be rewritten in terms of the empirical eigenfunctions ϕ_i and corresponding spectral coefficients a_i as

$$J(f) = \frac{1}{2}\sum_{i=1}^{M}(a_i(T) - a_i^T)^2 M_i + \frac{\epsilon}{2}\int_0^T f(t)^2\,\mathrm{d}t \tag{48}$$

where

$$a_i^T \equiv \frac{\int_\Omega (\boldsymbol{v}_T(\boldsymbol{x}) - \beta \boldsymbol{v}_r)\cdot \phi_i \, \mathrm{d}\Omega}{\int_\Omega \phi_i \cdot \phi_i \, \mathrm{d}\Omega} \tag{49}$$

Following the same procedure as that in Section 2.4, the objective function (Equation (48)) may be rewritten with the introduction of adjoint variables $\lambda_i(t)$ $(i = 1, 2, \ldots, M)$:

$$J(f) = \frac{1}{2}\sum_{i=1}^{M}(a_i(T) - a_i^T)^2 M_i + \frac{\epsilon}{2}\int_0^T f(t)^2 \, \mathrm{d}t + \sum_{k=1}^{M}\int_0^T \lambda_k(t) \times \frac{1}{M_k}\left[-\nu \sum_{l=1}^{M} a_l H_{kl} - \sum_{l=1}^{M}\sum_{m=1}^{M} a_l a_m Q_{klm} - \beta \sum_{l=1}^{M} a_l R_{kl} - \beta(\beta-1)C_k - N_k \frac{\mathrm{d}\beta}{\mathrm{d}t} + f(t) S_k \right] \tag{50}$$

Then the gradient of the objective function, ∇J, is found after integrating δJ by parts in time, and exploiting the initial conditions for $a_i(t)$ as follows:

$$\nabla J = \epsilon f(t) + \sum_{k=1}^{M} \frac{\lambda_k}{M_k} S_k \tag{51}$$

The adjoint variables $\lambda_j(t)$ $(j = 1, 2, \ldots, M)$ must then satisfy the following ordinary differential equations:

$$\frac{\mathrm{d}\lambda_j}{\mathrm{d}t} = \sum_{k=1}^{M} \frac{\lambda_k}{M_k}\left[\nu H_{kj} + \sum_{m=1}^{M} a_m Q_{kjm} + \sum_{l=1}^{M} a_l Q_{klj} + \beta R_{kj} \right] \quad (j = 1, 2, \ldots, M) \tag{52a}$$

with the following starting conditions at $t = T$:

$$\lambda_j(t = T) = (a_j(T) - a_j^T) M_j \qquad (j = 1, 2, \ldots, M) \tag{52b}$$

where M_j is defined by Equation (22). The gradient of the objective function, ∇J, given by Equation (51) is exploited in the conjugate gradient method of Fletcher and Reeves [11] to minimize the objective function (48). The sensitivity equation for this case is given by:

$$\frac{\mathrm{d}}{\mathrm{d}t}(\delta a_k) = \frac{1}{M_k}\left[-\nu \sum_{l=1}^{M} \delta a_l H_{kl} - \sum_{l=1}^{M}\sum_{m=1}^{M} \delta a_l a_m Q_{klm} - \sum_{l=1}^{M}\sum_{m=1}^{M} a_l \delta a_m Q_{klm} - \beta \sum_{l=1}^{M} \delta a_l R_{kl} + d(t) f S_k \right] \quad (k = 1, 2, \ldots, M) \tag{53a}$$

with the initial conditions

$$\delta a_k(t=0)=0 \qquad (k=1, 2, \ldots, M) \tag{53b}$$

Here, $d(t)$ is the conjugate direction which is updated in each iteration by the following rule

$$d^n(t)=\nabla J^n+\gamma^n d^{n-1}(t) \tag{54}$$

where

$$\gamma^n=\frac{\displaystyle\int_0^T(\nabla J^n(t))^2\,\mathrm{d}t}{\displaystyle\int_0^T(\nabla J^{n-1}(t))^2\,\mathrm{d}t} \tag{55}$$

with $\gamma^0=0$, and n is the iteration number. The value of ρ^n that minimizes $J(f^n-\rho^n a^n)$ is obtained, as previously, by differentiating $J(f^n-\rho^n a^n)$, with respect to ρ^n, and setting the resulting equation equal to zero.

$$\rho^n=\frac{\displaystyle\sum_{i=1}^{M}(a_i(T)-a_i^T)\delta a_i(T)M_i+\epsilon\int_0^T f^n(t)d^n(t)\,\mathrm{d}t}{\displaystyle\sum_{i=1}^{M}(\delta a_i(T))^2M_i+\epsilon\int_0^T d^n(t)^2\,\mathrm{d}t} \tag{56}$$

where $\delta a_i\,(T)$ is the value of δa_i at $t=T$, M_i is defined by Equation (22). The Fletcher–Reeves algorithm as applied to the optimal control problem employing the low dimensional dynamic model follows the procedure outlined below:

1. Assume $f(t)$ and calculate $a_k(t)$ $(k=1, 2, \ldots, M)$ using Equations (21a and b).
2. Solve the adjoint problem with appropriate terminal conditions (Equations (52a) and (52b)).
3. The gradient of the objective function, ∇J, is given by Equation (51).
4. The conjugate direction at the nth iteration is given by Equation (54), where γ^n is given by Equation (55).
5. Solve the sensitivity equation with the relevant initial conditions, i.e. Equations (53a and b).
6. Determine ρ^n that minimizes $J(f^n-\rho^n a^n)$ by Equation (56).
7. The optimal control is updated by

$$f^{n+1}(t)=f^n(t)-\rho^n d^n(t) \tag{57}$$

8. Repeat the above calculations until convergence.

3. RESULTS

In this section, we assess the accuracy and efficiency of the present method of solving the control problem of the Navier–Stokes equation employing the dimensional model obtained by

the Karhunen–Loève Galerkin procedure, as compared with the conventional method employing the original partial differential equation. For brevity of communication, we call the method employing the original partial differential equation the FDM-CG, while the method employing the low dimensional model is called the KLG-CG. In both methods, the minimization of the objective function has been done by means of the conjugate gradient method suggested by Fletcher and Reeves [11]. The following criterion is used to stop the iteration process of the conjugate gradient method:

$$J(f^{(i+1)}) - J(f^{(i)}) < \epsilon_1 \tag{58}$$

where J is defined by Equation (11), $f^{(i)}$ is the control at the ith iteration and ϵ_1 is a prescribed small number.

As with the first example, we consider the case where the target profile $\boldsymbol{v}_T(\boldsymbol{x})$ is given by Figure 2(b) with $\epsilon = 5 \times 10^{-5}$ in Equation (11). Figure 7 shows the convergence rate of the iteration procedure of both methods. We find that the value of the objective function decreases rapidly during the first couple of iterations. This figure also reveals that the convergence rate of the KLG-CG is slightly faster than that of FDM-CG.

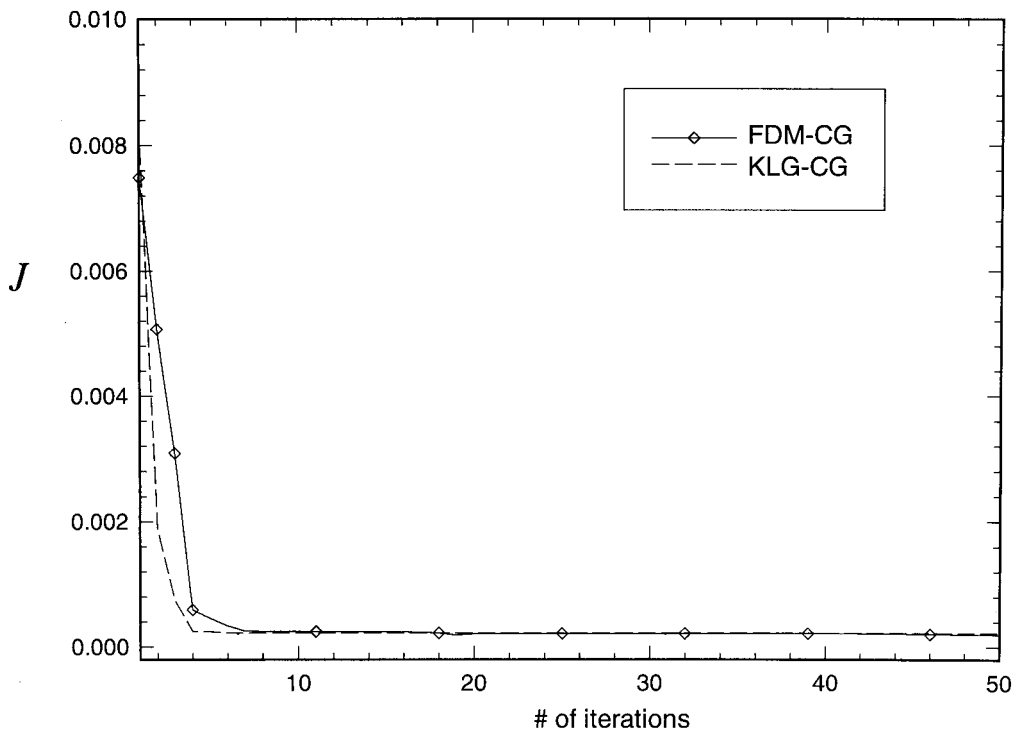

Figure 7. Convergence rate of conjugate gradient methods. The convergence rate of the KLG-CG is slightly faster than that of the FDM-CG.

Figure 8 depicts the optimal control $f(t)$ obtained by the KLG-CG in comparison with that by the FDM-CG. Also shown in the same figure is the original control $f(t)$ given by Equation (12a), which has been used to obtain the target velocity field $\boldsymbol{v}_T(\boldsymbol{x})$. As shown in Figure 8, the profile of optimal control obtained by the KLG-CG has almost the same shape as that by the FDM-CG, the energy of both of these optimal controls being much less than that of the original control given by Equation (12a). Figure 9 shows the states at the final time $t = T$, obtained by the FDM-CG (Figure 9(b)) and the KLG-CG (Figure 9(c)), which are indistinguishable from the target velocity field $\boldsymbol{v}_T(\boldsymbol{x})$ (Figure 9(a)).

The next example is the case where the target velocity field $\boldsymbol{v}_T(\boldsymbol{x})$ is given by Figure 3(b) and the value of ϵ in Equation (11) is 5×10^{-5}. The optimal control $f(t)$, obtained either by the KLG-CG, or by the FDM-CG, is shown in Figure 10, together with the original control, Equation (12b), which is employed to obtain the target $\boldsymbol{v}_T(\boldsymbol{x})$. This figure also shows that both the KLG-CG and the FDM-CG yield almost the same optimal trajectory of forcing $f(t)$, the energy of both of these optimal controls being much less than that of the original control employed to obtain the target velocity field.

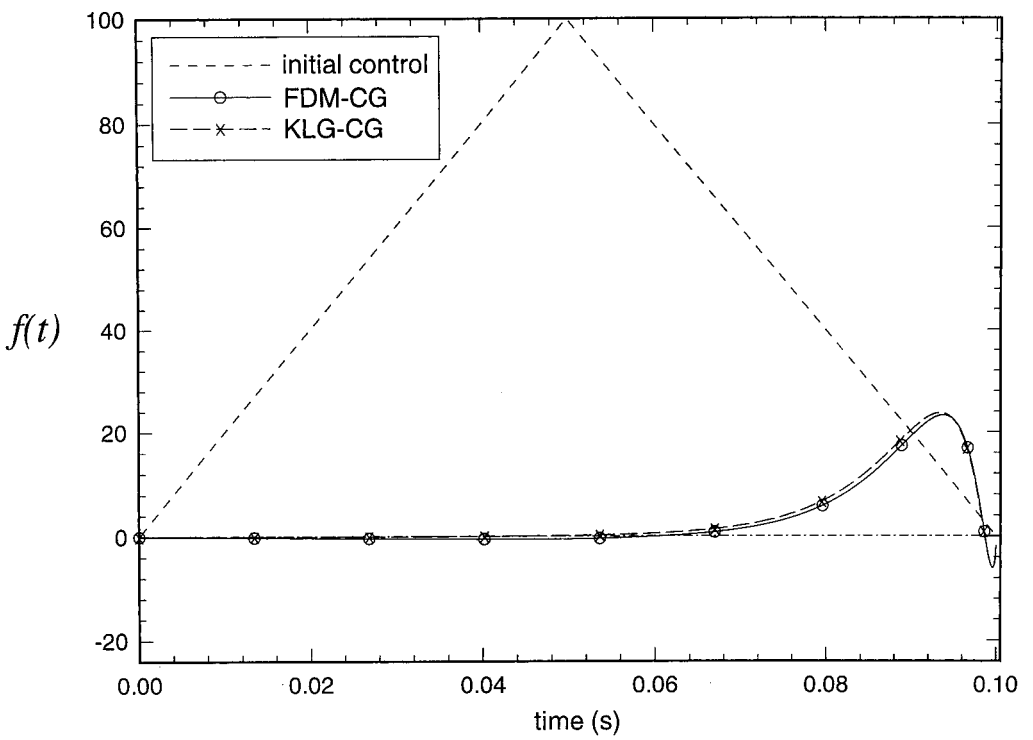

Figure 8. The profiles of the optimal control obtained either by the FDM-CG, or by the KLG-CG, for the target velocity field of Figure 2(b). The original control, Equation (12a), is also displayed for comparison.

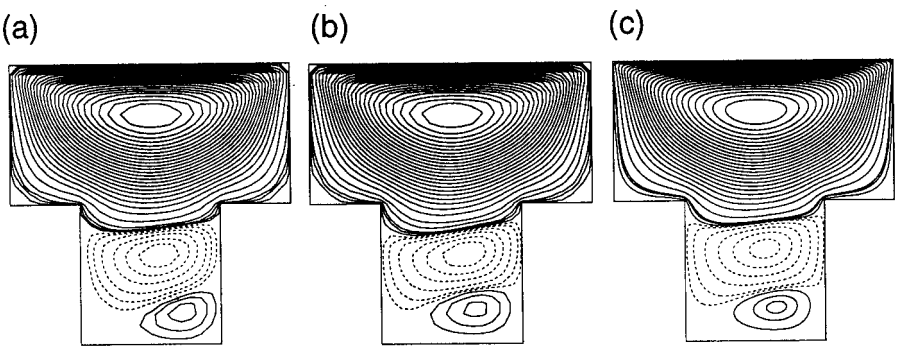

Figure 9. The comparison of the final state, $\boldsymbol{v}(\boldsymbol{x}, t = T)$, obtained either by the FDM-CG or by the KLG-CG, with the target velocity field $\boldsymbol{v}_T(\boldsymbol{x})$ given by Figure 2(b). These three velocity fields are virtually indistinguishable. (a) The target velocity field. (b) The final state obtained by FDM-CG. (c) The final state obtained by KLG-CG.

Figure 11 compares the transient flow fields when the control is given by Equation (12a) $f(t)$, which is employed to obtain the target $\boldsymbol{v}_T(\boldsymbol{x})$ of Figure 2(b), and when $f(t)$ is the optimal trajectory for the same target velocity field. Unless there is control action, there will be two counter-rotating vortices, a negative one in the upper region (drawn with solid lines) and the other one, which is positive in the lower region (drawn with dotted lines). However, because of the control action, a third negative vortex appears near the bottom. We may think that the energy of the control is somewhat proportional to the size of the third negative vortex near the bottom of the cavity. With the control given by Equation (12a) $f(t)$, the third vortex always exists from the very outset before it settle down to the target field, this consuming a large amount of energy. On the contrary, with the optimal $f(t)$, it only appears near the final time to fit the target field.

To quantify the results of the present study, we split the objective function defined by Equation (11) into two parts:

$$J = J_1 + \epsilon J_2 \tag{59a}$$

where

$$J_1 = \frac{1}{2}\int_\Omega (\boldsymbol{v}(\boldsymbol{x}, T) - \boldsymbol{v}(\boldsymbol{x}))^2 \mathrm{d}\Omega \tag{59b}$$

and

$$J_1 = \frac{1}{2}\int_0^T f(t)^2 \,\mathrm{d}t \qquad \text{with } T = 0.1 \tag{59c}$$

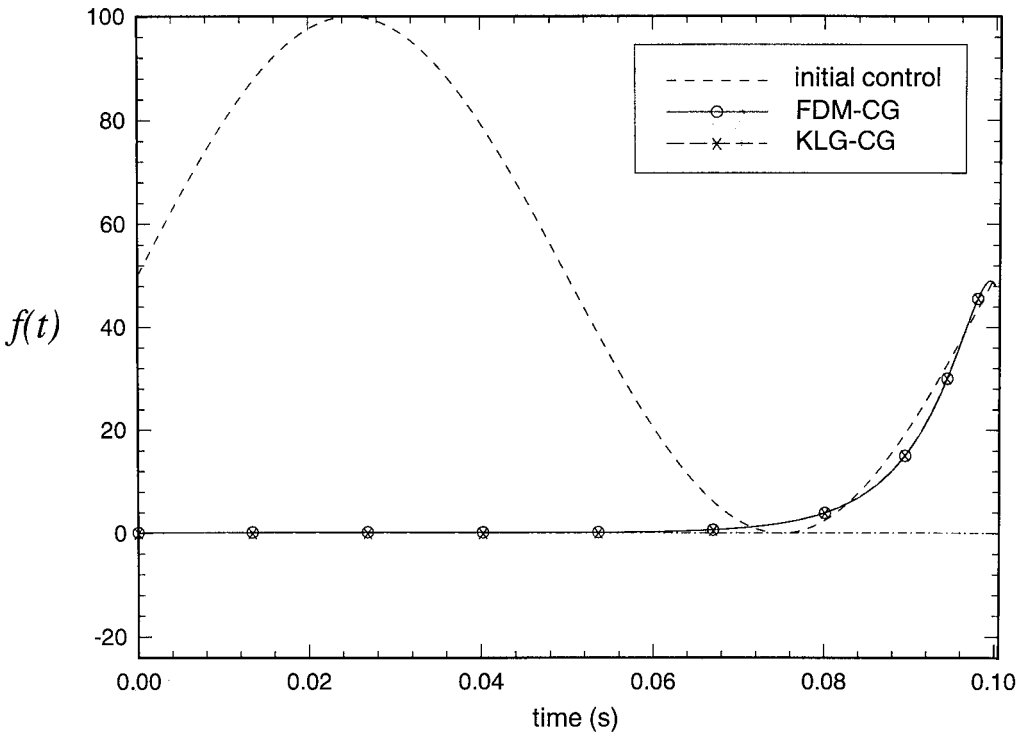

Figure 10. The profiles of the optimal control obtained either by the FDM-CG, or by the KLG-CG, for the target velocity field of Figure 3(b). The original control, Equation (12b), is also displayed for comparison.

Then J_1 measures the distance of the final state from the target and J_2 denotes the energy of the control. The magnitude of the parameter ϵ in Equation (59a) determines the relative importance of J_1 and J_2. For example, if the cost of control is expensive, we take larger values of ϵ.

Figure 12(a) and (b) show the variation of the optimal values of J_1 and J_2 with respect to ϵ when the target $\boldsymbol{v}_T(\boldsymbol{x})$ is given by Figure 2(b). As ϵ is increased, the value of J_1 for the optimal control increases, while the optimal value of J_2 decreases. In other words, as the importance of the cost of control, i.e. the ϵ value, increases, the distance between the final state $\boldsymbol{v}(\boldsymbol{x}, T)$ and the target $\boldsymbol{v}_T(\boldsymbol{x})$ becomes larger, but the energy of the control decreases when the optimal control is adopted in the system.

One of the most important results in the present investigation is the comparison of CPU time required to obtain the optimal control $f(t)$ by employing either the FDM-CG or the KLG-CG. When the ultrasparc workstation is used, one iteration of FDM-CG requires 24.94 min, while one iteration of KLG-CG requires only 4.2 s. The number of iterations needed to

$$f(t)\begin{cases} 2000t & (0\le t\le 0.05) \\ 2000(0.1-t) & (0.05\le t\le 0.1) \end{cases} \qquad f(t)= \text{optimal control}$$

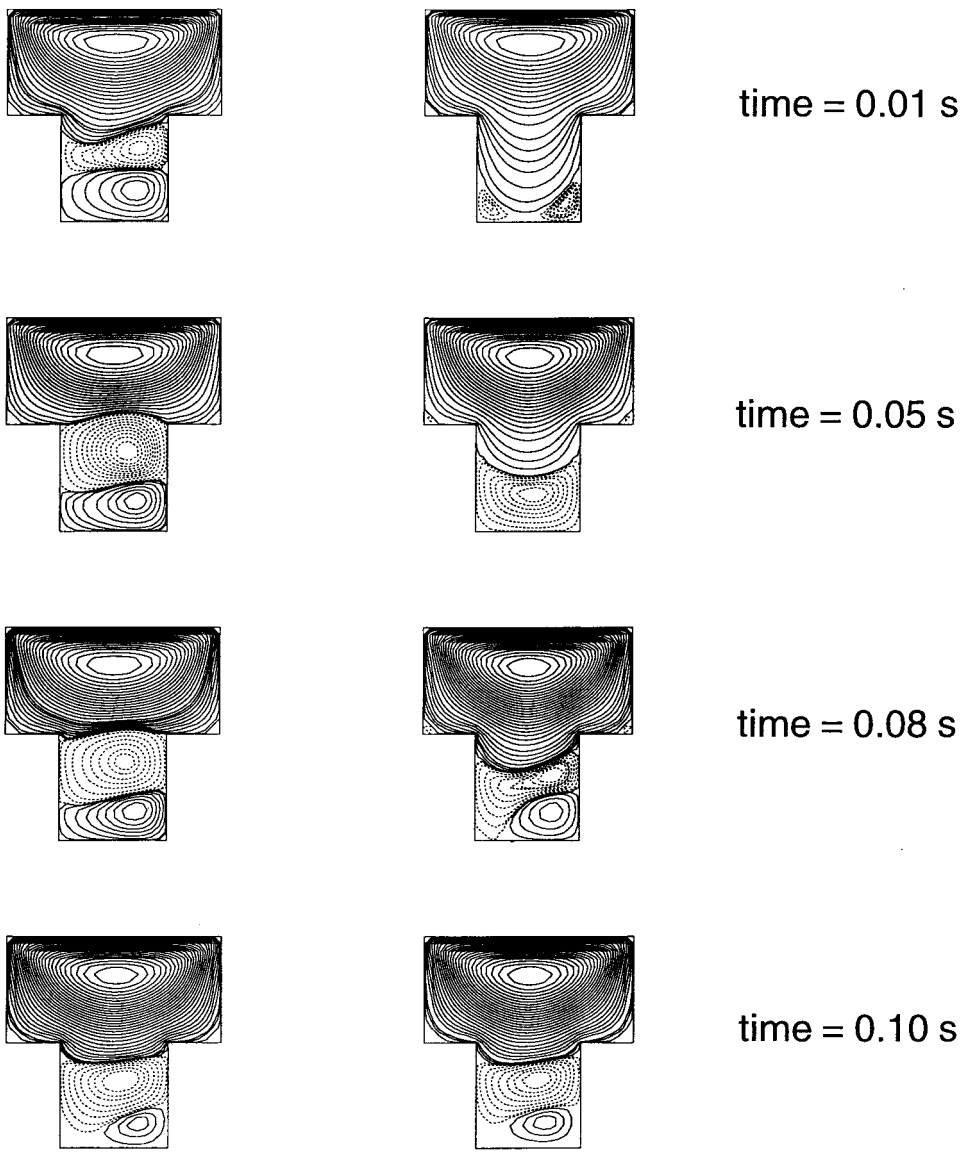

Figure 11. Comparison of the transient flow fields when $f(t)$ is given by Equation (12a) and $f(t)$ is the optimal control.

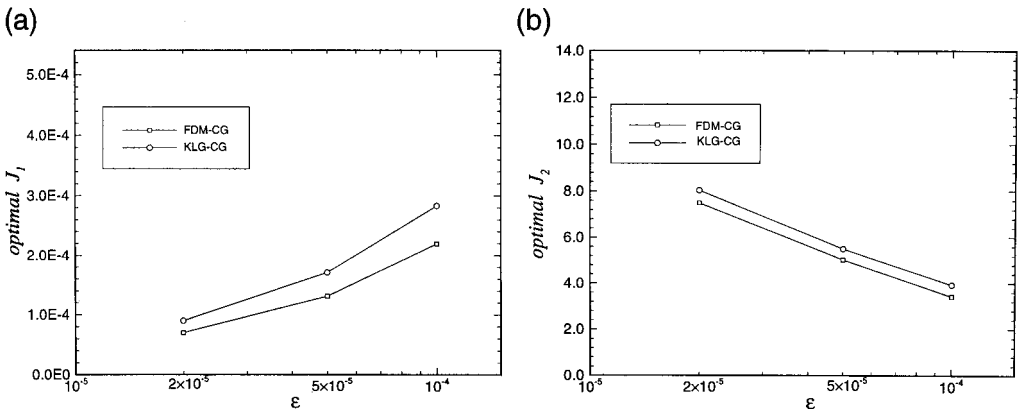

Figure 12. (a) The variation of the distance between the final state $\boldsymbol{v}(\boldsymbol{x}, T)$, and the target $\boldsymbol{v}_T(\boldsymbol{x})$, J_1, with respect to ϵ when the target velocity field is given by Figure 2(b). (b) The variation of the energy of the control, J_2, with respect to ϵ when the target velocity field is given by Figure 2(b).

reach the converged optimal profile is 100 for the FDM-CG, and 50 for the KLG-CG. Thus, the FDM-CG consumes 2485.7 min before yielding the optimal control profile. On the contrary, only 3 min 38 s, is needed for the KLG-CG to produce the same profile of optimal control. This drastic reduction on CPU time is easily expected from the fact that the degree of freedom of the low dimensional model is far less than that of the original partial differential equation. As the difference in the degree of freedom between the low dimensional dynamic models and the original partial differential equations shall become much larger as the dimensionality of the problem increases, the reduction of CPU time with the use for KLG-CG, instead of FDM-CG, shall be much more significant for three-dimensional problems.

4. CONCLUSION

The Karhunen–Loève Galerkin procedure is employed for the solution of optimal control problem of the Navier–Strokes equation. The objective function, which is determined by the distance between the final state $\boldsymbol{v}(\boldsymbol{x}, T)$ and the target velocity field $\boldsymbol{v}_T(\boldsymbol{x})$, along with the energy of the control, is minimized by using the conjugate gradient method. This method of solving the optimal control problem, called the KLG-CG in the present paper, has been compared with the traditional method employing the original partial differential equation (FDM-CG) in terms of accuracy and efficiency. The present investigation reveals that the KLG-CG yields profiles of optimal control as accurate as the FDM-CG, for various target velocity fields $\boldsymbol{v}_T(\boldsymbol{x})$ with several values of ϵ in Equation (11). As the degree of the freedom of the low dimensional dynamic model employed in the KLG-CG is much less than that of the original partial differential equation which is adopted in the FDM-CG, the KLG-CG yields accurate profiles of optimal control, with the consumption of much less CPU time, as

compared with the FDM-CG. This drastic reduction of CPU time will facilitate the real time implementation of many advanced control theories in various industrial processes.

Although the importance of control of fluid flow has been recognized for a long time, the development of rigorous, as well as practical, methodologies of flow control has been retarded because of the inherent mathematical complexities of the Navier–Strokes equations. In this regard, the Karhunen-Loève Galerkin procedure is suggested as an efficient method of solving problems of flow control, which is practical enough to be implemented in industrial processes, but is still keeping mathematical rigor.

REFERENCES

1. Park HM, Lee MW. An efficient method of solving the Navier–Strokes equation for the flow control. *International Journal of Numerical Methods in Engineering* 1998; **41**: 1131–1151.
2. Gunzburger MD, Hou L, Svobodny TP. Boundary velocity control of incompressible flow with an application to viscous drag reduction. *Siamese Journal of Control and Optimization* 1991; **30**: 167–181.
3. Abergel F, Temam R. On some control problems in fluid mechanics. *Theoretical Computing and Fluid Dynamics* 1990; **1**: 303–325.
4. Moin P, Moser RD. Characteristic-eddy decomposition of turbulence in a channel. *Journal of Fluid Mechanics* 1989; **200**: 471–506.
5. Park HM, Sirovich L. Turbulent thermal convection in a finite domain: Numerical results. *Physical Fluids A* 1990; **2**(9): 1659–1668.
6. Aubry N, Holmes P, Lumley JL, Stone E. The dynamics of coherent structures in the wall region of a turbulent boundary layer. *Journal of Fluid Mechanics* 1988; **192**: 115–173.
7. Deane AE, Kevrekidis IG, Karniadakis GE, Orszag SA. Low dimensional models for complex geometry flows: application to grooved channels and circular cylinders. *Physical Fluids* 1991; **3**: 23–37.
8. Moin P, Bewley T. Feedback control of turbulence. *Applied Mechanics Review* 1996; **47**(6, part 2): s3–s13.
9. Park HM, Cho DH. The use of the Karhunen–Loève decomposition for the modeling of distributed parameter systems. *Chemical Engineering Science* 1996; **51**: 81–98.
10. Park HM, Cho DH. Low dimensional modeling of flow reactors. *International Journal of Heat Mass Transfer* 1996; **39**(16): 3311–3323.
11. Fletcher R, Reeves RM. Function minimization by conjugate gradients. *The Computer Journal* 1964; **7**: 149–160.

